# PCL Detection Fundamentals

**Marco Martorella, Fabrizio Berizzi**
Department of Information Engineering
University of Pisa
Via Caruso 16, 56122 Pisa, Italy

m.martorella@iet.unipi.it, f.berizzi@iet.unipi.it

***ABSTRACT***

*Passive Coherent Location (PCL, or alternatively Passive Radar - PR) offers the ability to detect targets by using illuminators of opportunity. The principles of PCL are quite easy to understand as we can treat it as an active radar once the IO direct signal is acquired. Nevertheless, there are a number of issues that are specific to PCL that are not present in the case of active radar and that must be studied and dealt with when it comes to detecting targets. In these notes, fundamentals of detection for PCL are provided along with a number of signal processing techniques that have been developed to solve specific issues related to passive radar scenarios. This paper is to be considered as companion notes for the NATO Lecture on "PCL detection fundamentals" of the Lecture Series SET-243 on Passive Radar.*

## 1.0 INTRODUCTION

Passive bistatic radar (PBR) is gradually making progress, both in terms of signal processing and system development (demonstrators and prototypes). Several electromagnetic sources, i.e., illuminators of opportunity (IOs), can be used to implement such a radar system. Ground-based broadcast transmitters, such as frequency modulation (FM) and digital audio broadcasting (DAB) radio, as well as analogue and digital television have been largely exploited to demonstrate their capability to perform air and coastal surveillance [1-7]. Other IOs can also be found in space, where broadcast, navigation and communication systems continuously transmit towards the Earth. Such IOs can potentially enable PBR at a global scale.

A question that arises naturally is related to the effectiveness of passive radar when it comes to detecting targets and how this compares to active radar. Fundamental radar detection theory was laid in the early years of radar development and the same concepts can be applied to the PBR case. Therefore, optimality criteria and fundamental mathematical tools can still be exploited to address the detection problem for PBR.

Rather than repeating well known concepts, in these notes, we will concentrate on those differences and issues that arise when dealing with passive rather than active radar. More in details, we will recast the matched filter implementation, which is typical of active radar, into the problem of obtaining an equivalent result through the calculation of a cross-correlation function. The problem will be tackled in a two-dimensional space to account for both range and Doppler target's shifts. Efficient algorithms for the calculation of the two-dimensional cross-correlation function (2D-CCF) will be considered since this step is computationally very expensive.

The problems of direct signal and clutter cancellation will also be addressed that requires specific solutions that are typical of PBR. More specifically, we will look at a well-known solution, namely the Extensive Cancellation Algorithm (ECA) [8].

Finally, we will study the problem of reference signal cleaning, which is a necessary step to enable effective detection with PCL systems.

## 2.0 2D MATCHED FILTERING FOR PASSIVE RADAR

This section focuses on the implementation of two-dimensional matched filtering in the PBR case. Firstly, the equivalence between cross-correlation and matched filter will be addressed followed by the concept of two-dimensional cross-correlation function (2D-CCF). Efficient methods for the calculation of the 2D-CCF will be then introduced and discussed.

### 2.1 Equivalence between matched filter and cross-correlation

It can be easily shown that a matched filter (MF) can be implemented through the calculation of a cross-correlation. A matched filter is represented in Fig 2.1 where $s_R(t)$ represents the signal received by the passive radar through the surveillance antenna, $s_o(t)$ represent the signal at the output of the MF and $h_{MF}(t)$ represents the MF impulse response.

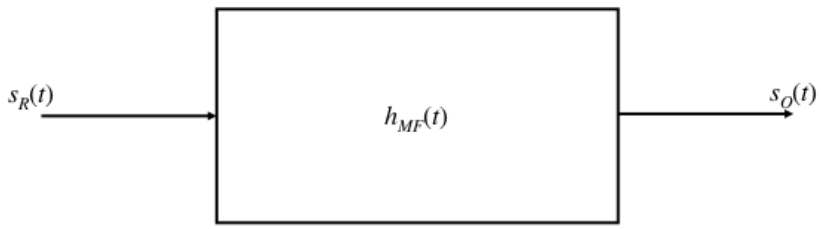


**Figure 2.1. Matched filter**

Eq. (1) shows the convolution operation that produces the output signal $s_o(t)$

$$s_o(t) = s_R(t) \otimes h_{MF}(t) = \int s_R(\tau)\, h_{MF}(t-\tau)\, d\tau \tag{1}$$

In order to define the MF impulse response, we need to know the transmitted signal waveform. As this is not generated by the radar itself a copy of the transmitted signal is obtained through the signal received by the PCL reference antenna, namely $s_{ref}(t)$. The MF impulse response is therefore obtained by means as follows:

$$h_{MF}(t) = s_{ref}^*(-t) \tag{2}$$

Therefore, by substituting (2) in (1), we obtain

$$s_o(t) = s_R(t) \otimes h_{MF}(t) = \int s_R(\tau)\, s_{ref}^*(\tau - t)\, d\tau \tag{3}$$

Which shows that the same output signal can be obtained by cross-correlating the input signal with the reference signal. This equivalence directly suggests how to implement a MF in the case of a PCL system. A pictorial view is given in Fig. 2.2.

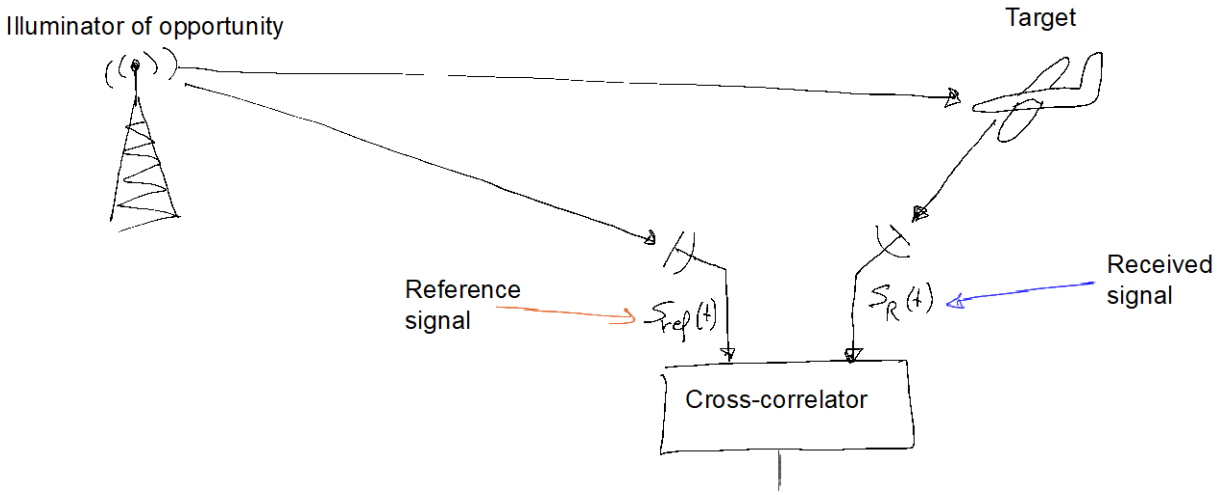


**Figure 2.2. Matched Filter implementation for a PCL system via a cross-correlation**

## 2.2 2D-CCF

The MF defined in Section 2.1 does not take into account Doppler shifts. If a target moves, it can be shown that a Doppler shift is generated. Therefore, a MF must take this into account in order to match the signal at its input. Equivalently, the cross-correlation function must do the same by introducing another variable that accounts for the Doppler shift. This can be done by extending the 1D-CCF to the 2D-CCF, as follows:

$$CCF(\tau,\nu) = \int s_R(\tau)\, s_{ref}^*(\tau - t)\, exp(-j2\pi\nu t)\, d\tau \quad \textbf{(4)}$$

Where $\nu$ represents the Doppler shift. Eq. (4) can be read as a cross-correlation between a Doppler shift compensated version of the received signal and the reference signal. As it will be clear in the next subsections, different interpretations of the 2D-CCF lead to different efficient implementations of its calculation.

It is also important to note that the 2D-CCF is a two-dimensional function with a supporting domain represented by delay-time and Doppler. As the delay-time can directly be transformed into bistatic range, we can conclude that the 2D-CCF can be interpreted as a bistatic range-Doppler map.

As signals are sampled and digitised eq. (4) should be represented by using a numerical representation, as follows:

$$CCF(l,m) = \sum_{n=0}^{N-1} s_R(n)\, s_{ref}^*(n-l)\, exp\left(-j2\pi\frac{mn}{N}\right) \quad \textbf{(4)}$$

Where *n* represents the time, *l* represents the delay-time and *m* represents the Doppler shift. The total number of time samples is set to *N*, which depends on the Coherent Processing Interval (CPI) considered and the system sampling rate ($T_S$), as follows:

$$N = \frac{CPI}{T_S} = CPI \cdot F_S \quad \textbf{(5)}$$

Where $F_S = {}^1/_{T_S}$.

An example of 2D-CCF is shown in Fig. 2.3. This visualisation result is often addressed as bistatic range-Doppler map. The axes refer to bistatic range and bistatic Doppler.

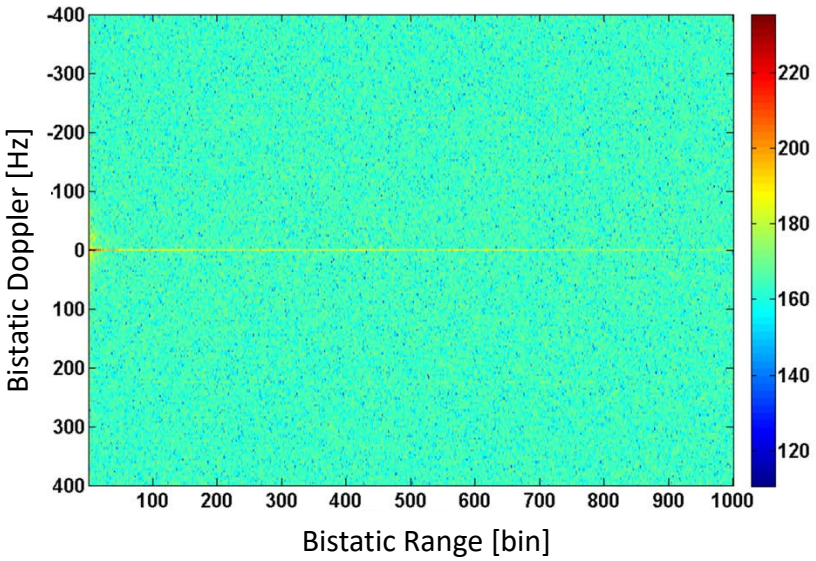


**Figure 2.3. Bistatic range-Doppler map**

## 2.3 Efficient calculation of 2D-CCF

The PCL received signals, both surveillance and reference, are sampled based on the signal bandwidth (*B*). Therefore, in order to satisfy Nyquist condition, signals should be sampled at a frequency that is not smaller than *B*. As typical IOs transmit continuously and everywhere, CPIs can be made long in order to obtain a high integration gain and therefore improve the SNR. As an example, we may consider a DVB-T signal channel, which has a bandwidth roughly equal to 8 MHz and a CPI of 1s. In this case, N = 8 million samples. The calculation of a cross-correlation function for a for a number of range bins M = 1000 and a number of Doppler bins D = 1000, would lead to a number of complex multiplication equal to N*M*D = 8 trillion multiplications.

It is clear that the computational load is not to be neglected and that some ways of reducing this computational burden must be found. In the following subsections we will be looking at two exact methods, namely the correlation FFT and the Direct FFT, and an approximated method, namely the batched algorithm.

### 2.3.1 Correlation FFT

The correlation FFT method derives from an interpretation of eq. 4. In fact by simply swapping the position of the exponential function and the reference signal we obtain:

$$CCF\,(l,m) = \sum_{n=0}^{N-1} s_R\,(n)\,exp\left(-j2\pi\frac{mn}{N}\right) s_{ref}^{*}\,(n-l) \qquad \textbf{(6)}$$

By substituting (7) into (6) we obtain a new expression that shows that the 2D-CCF can be calculated as the 1D cross-correlation of a Doppler shift compensated signal, namely $s_R(n,m)$, and the reference signal. It should be noted that the latter signal depends also on *m*, which represents the Doppler shift.

$$s_R(n,m) = s_R(n)\, exp\left(-j2\pi \frac{mn}{N}\right) \quad \textbf{(7)}$$

$$CCF(l,m) = \sum_{n=0}^{N-1} s_R(n,m)\, s_{ref}^*(n-l) \quad \textbf{(8)}$$

Cross-correlations can be calculated efficiently in the Fourier domain. In particular, we note that

$$CCF(l,m) = IDFT\left[S_R(k,m)\, S_{ref}^*(k)\right] \quad \textbf{(9)}$$

Where

$$S_R(k,m) = DFT\left[s_R(n,m)\right] \quad \textbf{(10)}$$

$$S_{ref}(k) = DFT\left[s_{ref}(n)\right] \quad \textbf{(11)}$$

It is also interesting to note that the DFT of $s_R(n,m)$ must be calculated only once (for instance for $m = 0$) as, for any other value of $m$, it can be obtained by means of a simple shift. Therefore, in terms of computational load

- two N-points FFT must be calculated at the beginning and only once
- at each iteration, N complex multiplications and one IFFT must be calculated.

This can be expressed with the standard notation used to evaluate the computational effort:

$$O_{CF} = 2Nlog_2(N) + N_f\left[N + Nlog_2(N)\right] \quad \textbf{(12)}$$

### 2.3.2 Direct FFT

The Direct FFT method can be derived by interpreting (4) as the DFT of the product of two signals, as follows:

$$CCF(l,m) = DFT\left[s_R(n)\, s_{ref}^*(n-l)\right] \quad \textbf{(13)}$$

With this method, no initial FFT must be calculated and at each interation N complex multiplications have to be calculated along with an FFT. In terms of standard notation, this can be expressed as follows:

$$O_{DF} = N_\tau\left[N + Nlog_2(N)\right] \quad \textbf{(14)}$$

The difference in terms of computational load between the two approaches lies on the number of iterations to be completed as, for each iteration, they have the same number of operations. The number of iterations in the correlation FFT method is related to the number of range cells ($N_\tau$) of the range-Doppler map that must be obtained, whereas the number of iterations that are required for the direct FFT method is related to the number of Doppler cells ($N_f$) that must be displayed in the range-Doppler map.

Therefore, in those cases where the number of bistatic range bins are greater than the number of Doppler bins, the direct FFT method is to be preferred and viceversa. Fig. 2.4 shows a pictorial view that explain this concept.

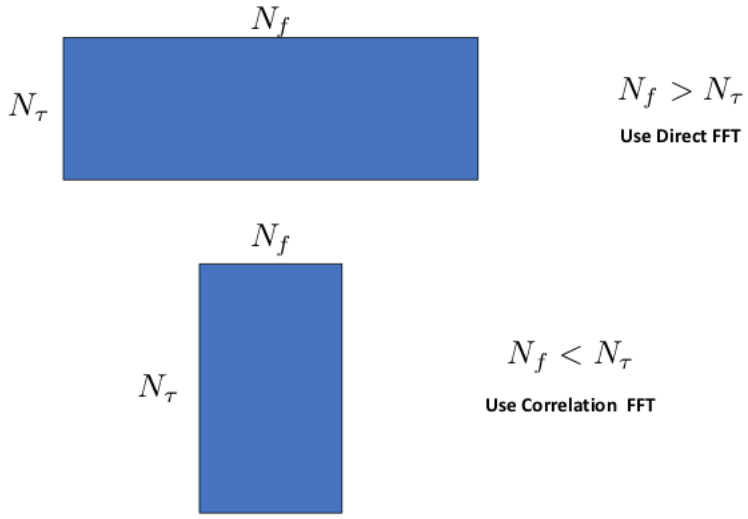


**Figure 2.4. Correlation FFT vs Direct FFT**

## 2.4 Batches algorithm

Both direct and correlation FFT methods may be still computationally too expensive. This is due to the fact that both techniques optimise the calculation only along one dimension, either range or Doppler. In fact the correlation FFT method allows for the number of Doppler cells to be selected but it calculates the output for all range bins even though only a limited amount of range bins are of interest (mainly due to the radar range coverage). On the other hand, the direct FFT method allows for the range bins to be selected but it calculates the output for all Doppler bins, including those that correspond to very high Doppler frequencies and therefore to those target's velocities that are physically impossible to reach.

Unfortunately, there is no method that produces an exact solution and at the same time allow for both range and Doppler bins to be selected. Nevertheless, a method, namely the batches algorithm, has been proposed that allows for range and Doppler bins to be selected at the expenses of a small SNR loss but with a very large computational load reduction. It should be mentioned that other techniques have been proposed that aim at achieving the same result, such as the channelization technique [8].

The batches algorithms is implemented by means of a subdivision of both the reference and surveillance signals into segments (batches). A pictorial view of this segmentation is given in Fig 2.5.

In mathematical terms, this can be represented by rewriting eq. (4) as follows:

$$CCF\left(l,m\right)=\sum_{r=0}^{n_B-1}\exp\left(-j2\pi\frac{mrN_B}{N}\right)\cdot\sum_{p=0}^{N_B-1}s_R\left(rN_B+p\right)s_{ref}^{*}\left(rN_B+p-l\right)\exp\left(-j2\pi\frac{mp}{N}\right) \quad \textbf{(15)}$$

Where $n_B$ is the number of batches and $N_B$ is the batch length and where $n_B \cdot N_B = N$.

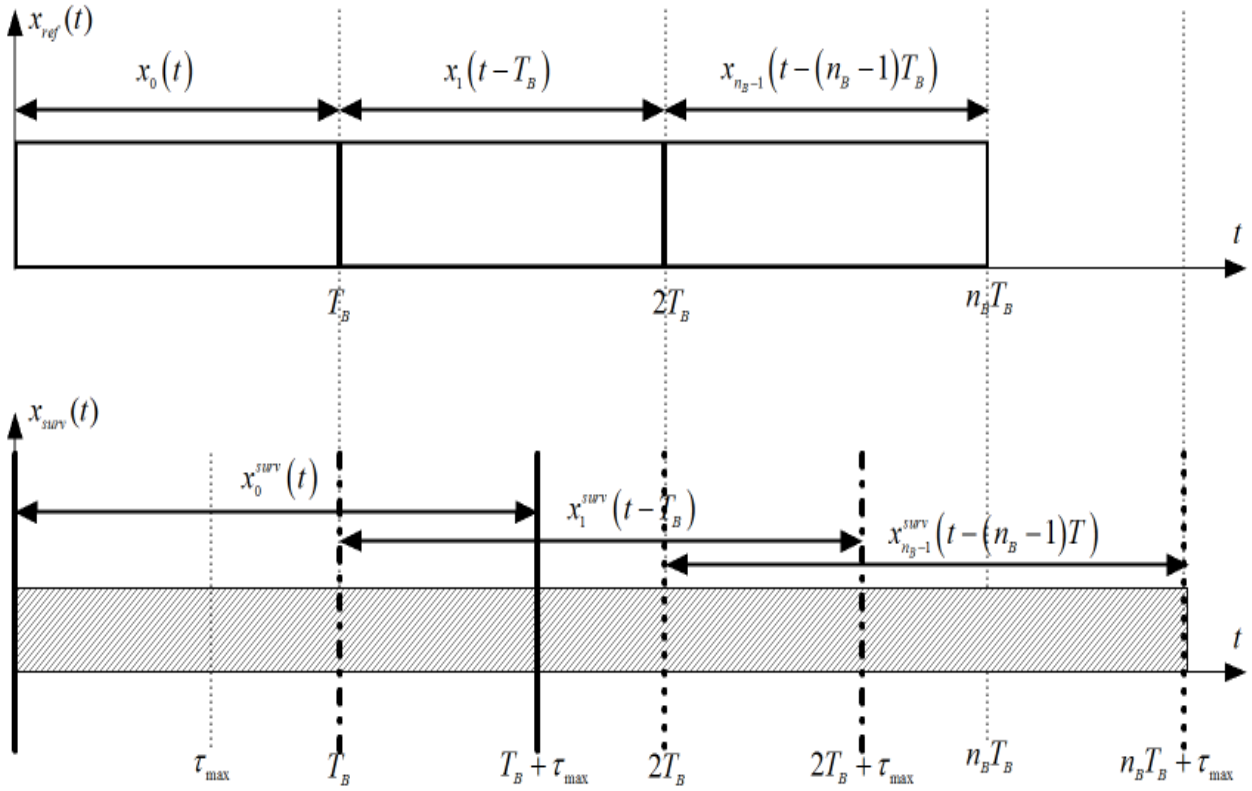


**Figure 2.5. Batches algorithm - Signal segmentation**

The assumption that is made for the bacthes algorithms to be effectively applied is that the Doppler effect within one batch is neglectable, which means that the phase rotation induced by the complex exponential function within the second sum can be ignored. Therefore, eq. (15) can be approximated as follows:

$$CCF(l,m) = \sum_{r=0}^{n_B-1} \exp\left(-j2\pi \frac{mrN_B}{N}\right) \sum_{p=0}^{N_B-1} s_R(rN_B+p)\, s_{ref}^*(rN_B+p-l) \tag{16}$$

The approximation made in (16) can be represented as a step-wise phase function rather than a linear function, as shown in Figure 2.6.

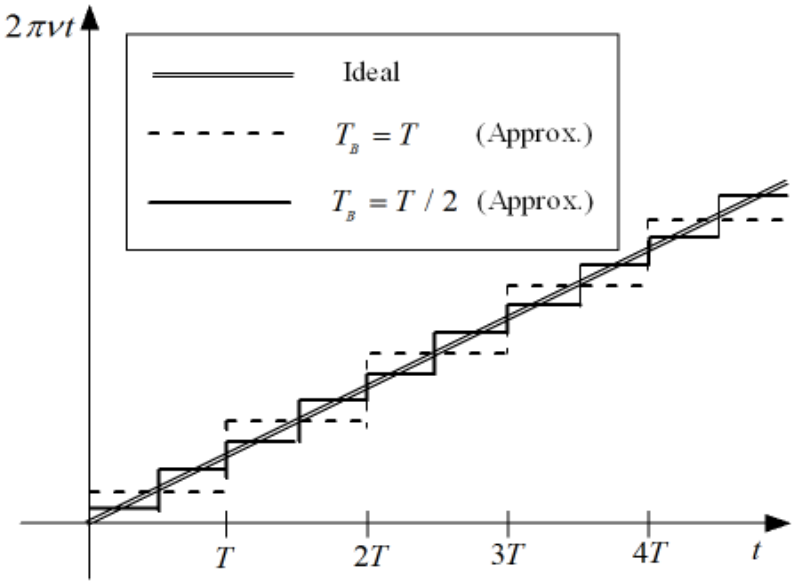


**Figure 2.6. Batches algorithm – Phase approximation**

For the sake of clarity, we may rewrite eq. (16) as follows:

$$CCF\,(l,m) = \sum_{r=0}^{n_B-1} CCF(l,r)\exp\left(-j2\pi\frac{mrN_B}{N}\right) = DFT\,[CCF\,(l,r)] \tag{17}$$

Where *CCF* (*l*, *r*) is the 1D-CCF calculated for the *r*-th batch and the *CCF* (*l*, *m*) is obtained as a DFT of along the *r*, which represents a sort of slow-time domain. This processing scheme is similar to that of a FMCW radar, where each batch can be associated with a FMCW ramp. Figure 2.7 represents a flow chart of the batches algorithms processing scheme.

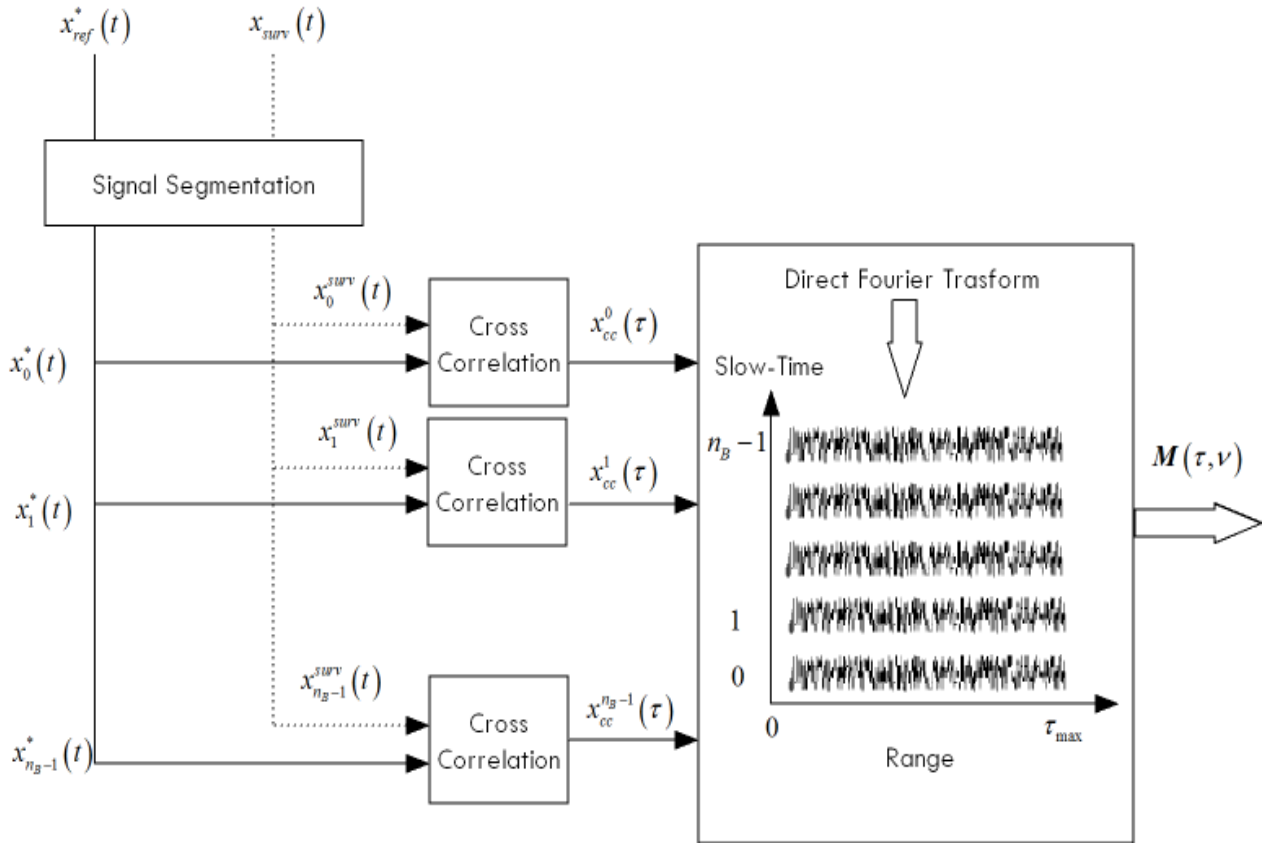


**Figure 2.7. Batches algorithm – Signal processing scheme**

In order to evaluate the SNR losses that are introduced by the approximation in (16) and shown in Fig. 2.6, we will make the following considerations. Longer batches will produce a smaller number of batches. Consequently, the DFT will be calculated over a smaller number of points, therefore reducing the computational load. On the other hand, longer bathes will introduce a larger error in the phase approximation and therefore heavier losses in terms of SNR due to Dopper phase rotation that would not be compensated. Shorter batches, instead, would produce a larger number of batches and therefore the DFT would have to be calculated over a larger number of points, therefore increasing the computational load. Conversely, the phase errors would be smaller and therefore the SNR losses would be smaller. An extensive analysis of the losses introduced by the batches algorithm has been shown in [9]. Results obtained from real data collected with a passive radar demonstrator owned by the Italian National Consortium for Telecommunications (CNIT) are shown in Fig. 2.8. It is quite clear from the plots that losses increase when the target-induced Doppler is higher and when the batch is longer. The plots in Figure 2.8 also show the theoretical losses (solid line), which are matched by real data. The computational load for the four cases is shown in Table 2.1.

| Batch Length | Processing Time |
|---|---|
| 31.28 μs | 4.93s |
| 218.76 μs | 0.92s |
| 333.29 μs | 0.71s |
| 924 μs | 0.59s |

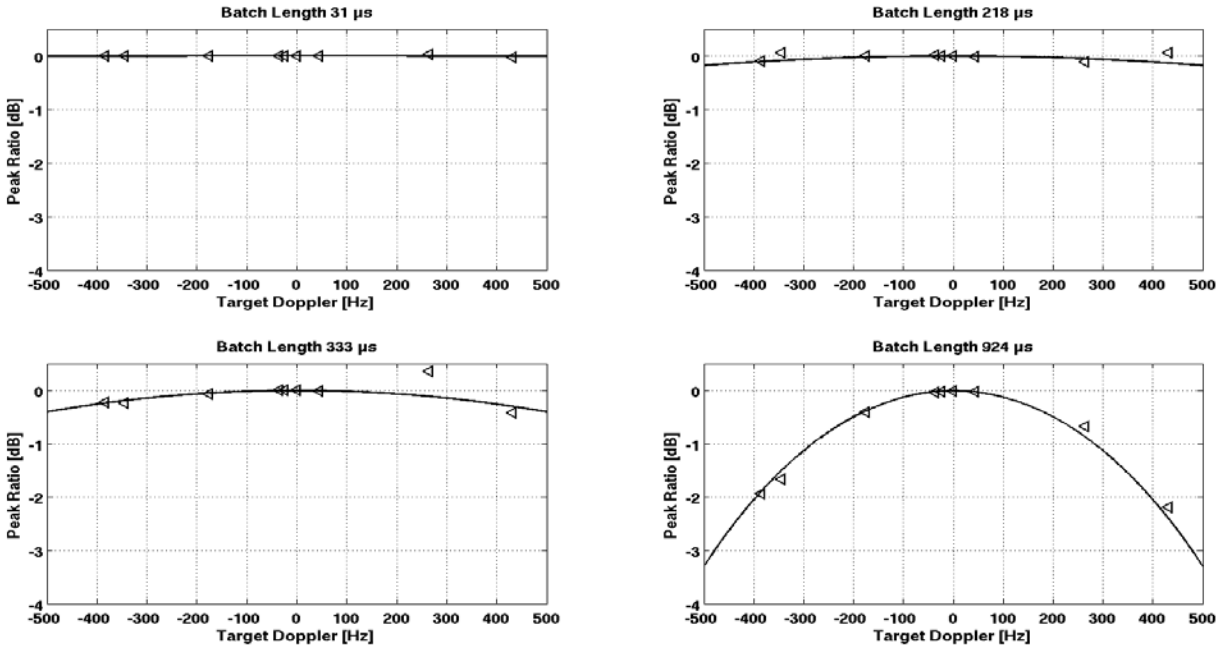


**Figure 2.8. Batches algorithm – Signal processing scheme**

## 3.0 DIRECT SIGNAL AND CLUTTER CANCELLATION

The signal received from the surveillance antenna contains the echoes from the targets that are illuminated by the e.m. source of opportunity. Unfortunately, this is not the only component that is present in the received signal. In fact the same signal that is emitted by the IO may propagate directly to the surveillance antenna and be captured by an antenna sidelobe. Although sidelobes attenuate the signal significantly with respect to the main lobe, the direct signal may be tens of dBs stronger than any target's echo. Therefore, the direct signal component is by far the strongest signal that is received by the surveillance antenna. Such component is constrained at zero bistatic range and at zero Doppler and when both the IO and the surveillance antenna are stationary. Although the stationarity and the zero-range position of the direct signal response in the 2D-CCF (range-Doppler map), the strength of this signal ripples out to reach other range-Doppler cells and thererfore masks targets that may be positioned at other range and Doppler cells.

Clutter is also present in PCL as it is in active radar. Nevertheless, it should be noted that, due to the bistatic geometry and in particular in the forward or quasi-forward scatter region, clutter can be very strong and appear at several bistatic range cells. This effect, combined with the direct signal effect, may mask several targets and prevent their detection.

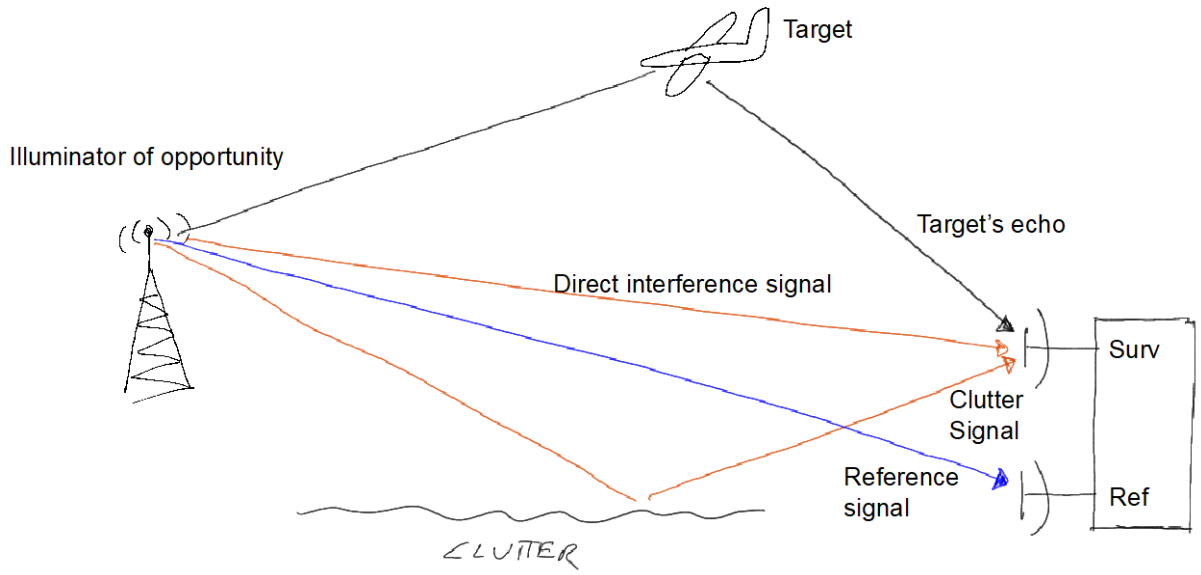


**Figure 3.1. PCL scenario – Direct and multipath signal interference**

A complete model for the received signal is shown in eq. (18), where the first term represents the direct signal component, the second term (first sum) represents the target's echoes, the third term (second sum) represents the clutter and the last term is noise component.

$$s_R(t) = A_R s_T(t) + \sum_{m=1}^{N_T} a_m s_T(t - \tau_{T_m}) \exp(j2\pi f_{D_m} t) + \sum_{i=1}^{N_s} b_i s_T(t - \tau_{c_i}) + n(t) \quad \textbf{(18)}$$

In order to maximise detection performances, both the direct signal and the clutter components must be removed or at least strongly attenuated. In the next sub-section, we will look at a well-known technique that goes in that direction.

## 3.1 Extensive Cancellation Algorithm

The Extensive Cancellation Algorithm (ECA) consists of a projection of the received signal onto a sub-space that is orthogonal to the disturbance sub-space [8]. As the disturbance signals (direct signal and clutter) are much stronger than the target's echoes, it can be argued that the subspace occupied by them can be easily estimated by considering such signal as replicas of $s(t)$. In its most simple form, the ECA, considers only stationary replicas, which correspond to zero-Doppler contributions. More complex versions of the ECA also include the case of non-zero-Doppler clutter, such as the ECA batches and ECA batches and stages.

A reasonable assumption can be made in order to reduce the computational load that is required by the ECA technique, which consists of limiting the number of range cells where significant clutter contribution is concentrated. Closer bistatic range cells are in the forward and near forward scatter region and they also at a closer distance from the transmitter and the receiver. Both conditions have the effect of producing a high level of clutter compared to cell at further bistatic ranges. If this assumption can be made, then we can limit the signal analysis to the first K bistatic range cells.

To derive the ECA algorithm, *N* samples of the surveillance signal are considered

$$\mathbf{s}_R = [s_R[0], s_R[1], ..., s_R[N-1]] \quad \textbf{(19)}$$

Along with *N*+*R*-1 samples from the reference channel

$$\mathbf{s}_{ref} = [s_{ref}[-R+1], s_{ref}[0], s_{ref}[1], ..., s_{ref}[N-1]] \quad \textbf{(20)}$$

Where *R*-1 is the number of additional reference samples to be considered to obtain a desired integration, which in this case would be equal to *N* over *R* time bins.

In order to obtain a cancellation of the clutter, the following optimisation problem must be solved, where we aim at minimising the residual energy after removing the clutter from the first K range cells.

$$\min_{\alpha} \left[ \|\mathbf{s}_R - \mathbf{X}\alpha\|^2 \right] \quad \textbf{(21)}$$

Where

$$\mathbf{X} = \mathbf{B}\mathbf{S}_{\mathbf{ref}}\mathbf{B} \quad \textbf{(22)}$$

And B is a matrix that selects only the last *N* rows of

$$\mathbf{S}_{ref} = \begin{bmatrix} \mathbf{s}_{ref} & \mathbf{D}\mathbf{s}_{ref} & \mathbf{D}^{\mathbf{2}}\mathbf{s}_{ref} & \dots & \mathbf{D}^{\mathbf{K-1}}\mathbf{s}_{ref} \end{bmatrix} \quad \textbf{(23)}$$

Where **D** is a delay matrix that simply shifts the reference signal by one time sample. It should be noticed that the columns of matrix in (23) define a basis for a K-dimensional disturbance subspace. The solution for eq. (21) is the standard solution of a Lease Square Error problem, which can be found in (24)

$$\boldsymbol{\alpha} = \left(\mathbf{X}^H\mathbf{X}\right)^{-1}\mathbf{X}^H\mathbf{s}_R \quad \textbf{(24)}$$

Therefore, the clutter-free signal can be obtained as follows

$$\mathbf{s}_{ECA} = \mathbf{s}_R - \mathbf{X}\boldsymbol{\alpha} = \left[\mathbf{I}_N - \mathbf{X}^H\mathbf{X}^{-1}\mathbf{X}^H\right]\mathbf{s}_R = \mathbf{P}\mathbf{s}_R \quad \textbf{(25)}$$

Where **P** is a projection matrix that projects the received signal onto the subspace orthogonal to the disturbance subspace.

Figures 3.2 and 3.3 show a real data range-Doppler map before and after the application of the ECA filter.

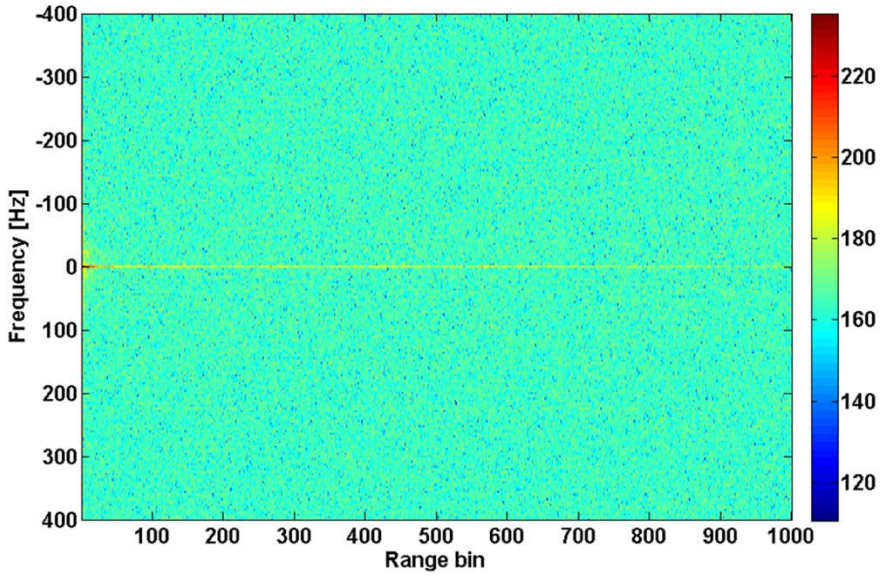


**Figure 3.2. Range Doppler map before ECA**

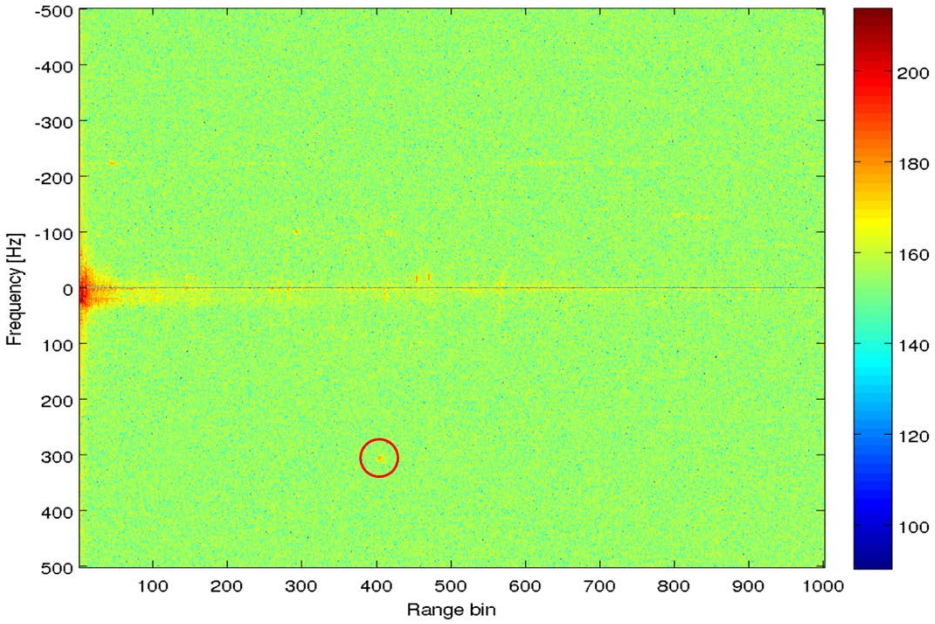


**Figure 3.3. Range Doppler map after ECA**

## 4.0 REFERENCE SIGNAL CLEANING

The ECA works effectively when the reference signal is perfectly known. As the reference signal is directly received by the passive radar antenna, we have to assume that such a signal is a perfect replica of the transmitted signal. Unfortunately, multipath effects are present also in the reference signal. Therefore, the signal received by the reference antenna is not a perfect replica of the transmitted signal. A realistic model of the reference signal is shown in (26)

$$s_{ref} = A_{ref}\, d(t) + \sum_{m=1}^{N_M} A_m d\left(t - \tau_m\right) + n_{ref}(t) \tag{26}$$

Where, $A_{ref}$ is the complex amplitude of the direct signal, $A_m$ are the complex weighs of the multipath components, $\tau_m$ are the delays of each multipath component and $n_{ref}(t)$ is the noise component.

Two methods will be described in the following subsections. One that is specific for analogue modulations and one that is specific for digital modulations.

### 4.1 Constant Modulus Algorithm

This method, namely the Constant Modulus Algorithm (CMA) is defined for generic analogue-modulated signals [8]. Such an algorithm is effective when several degrees of freedom are available both in the time and space domain. Nevertheless, CMA can be applied to either in the time-only and space-only dimensions. In these cases, the CMA is usually addressed as T-CMA for the time-only version and S-CMA for the space-only version.

The goal is to suppress additive interference (multipath) by constraining the output to be constant in modulus. This corresponds to minimising the following function

$$\hat{y}[n] = \min_{y[n]} \left\{ E\left[ \left( |y[n]|^2 - 1 \right)^2 \right] \right\} \tag{27}$$

Which leads to the solution in (28)

$$y[n] = \sum_{m=0}^{M-1} \sum_{l=0}^{L-1} w_{m,l}[n]\; s_{ref,m}\left[n - l\right] \tag{28}$$

Where *m* represents the spatial element index, *l* is the temporal sample index $s_{ref,m}$ is the reference signal collected by the *m*-th element and

$$w_{m,l}\left[n+1\right] = w_{m,l}\left[n\right] - \mu\epsilon[n] s^*_{ref}\left[n - l\right] \tag{29}$$

With

$$\epsilon[n] \triangleq \left\{ |y[n]|^2 - 1 \right\} \cdot y[n] \tag{30}$$

And where $\mu$ is a parameters that serves the purpose of trading accuracy for convergence speed.

## 4.2 Digital signal reconstruction and equalisation

In this section we will introduce two techniques to improve the reference signal when the transmitted signal is a digital one. In particular we will show that

- multipath can be removed by demodulating and remodulating the received signal to reproduce a perfect copy of the transmitted signal
- spurious peaks due to pilot sequences can be removed through an equalisation process.

### 4.2.1 Digital signal reconstruction

Some digital transmissions, such as DVB-T, offer the possibility to reconstruct the transmitted signal after demodulating and re-modulating the received signal. Part of this operation, and more specifically the demodulation, is typical of any DVB-T receiver, which aims at decoding the QAM symbols that represent the information content of DVB-T transmissions. Once such symbols are obtained, a perfect copy of the nominal transmitted signal can be obtained. Fig. 3.4 shows an example of DVB-T symbols demodulated in the presence of multipath and in absence of it.

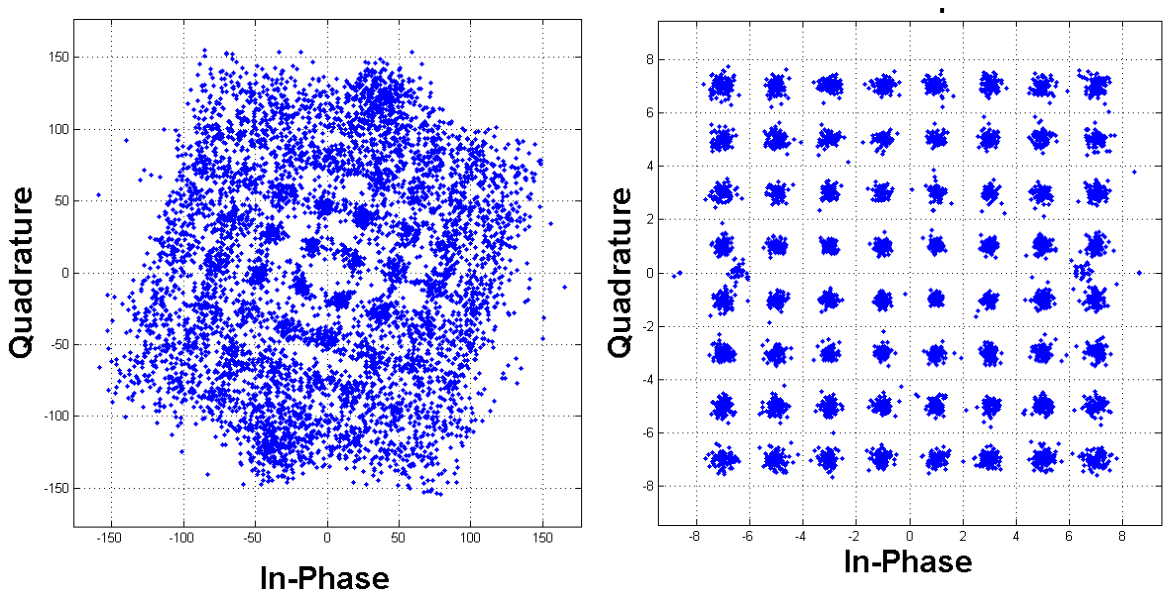


**Figure 3.4. Decoded symbols before and after**

We have to mention here that the re-modulated signal does not bear the distortions that may be introduced by the transmitter power devices. Such distortions, if known, have to be replicated in order to produce a signal that is as close as possible to the transmitted signal.

An example autocorrelation function (ACF) is presented in Fig. 3.5, where the ACF before and after signal reconstruction are shown in green and red colour, respectively. Two strong multipath components are visible at around 6 and 8 microseconds. The cross-correlation between the reconstructed and non-reconstructed reference signals is also shown in blue colour. The latter shows what would happen when multipath components are present in the reference signal. In fact, two peaks would appear in the CAF creating two target ghosts, which would produce two false alarms.

### 4.2.2 Digital signal equalisation

In addition to removing multipath, digital signal can be equalised to perform ACF shape control. An undesired effect is provoked by the presence of pilot sequences, which generate spurious peaks in the ambiguity function. An example of such spurious peaks is presented in Fig. 3.5, where an ambiguity function is shown relatively to some measured DVB-T signals.

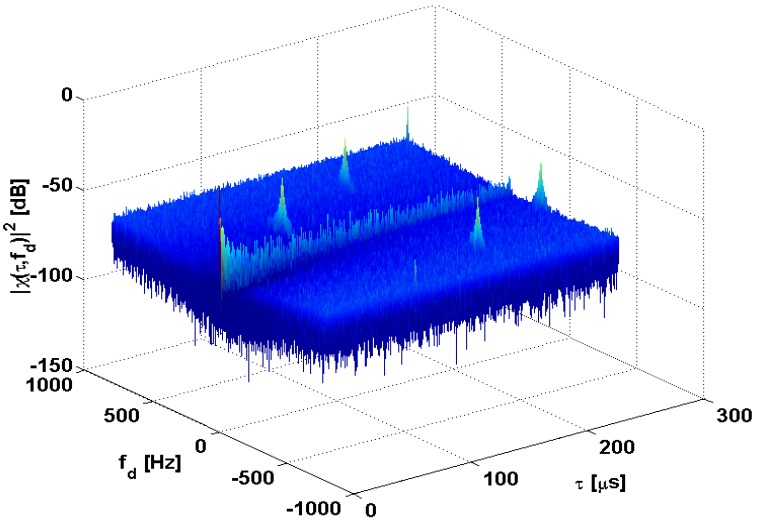


**Figure 3.5. Ambiguity Function – DVB-T signal – Presence of spurious peaks due to pilot sequences**

An effective algorithm can be implemented that aims at generating locally the Power Spectrum Density (PSD-Fourier Transform of the Autocorrelation Function) and perform an equalisation by generating a filtering function that aims at transforming the ACF into a spurious-free version of it. Details of the algorithm are shown in Fig. 3.6.

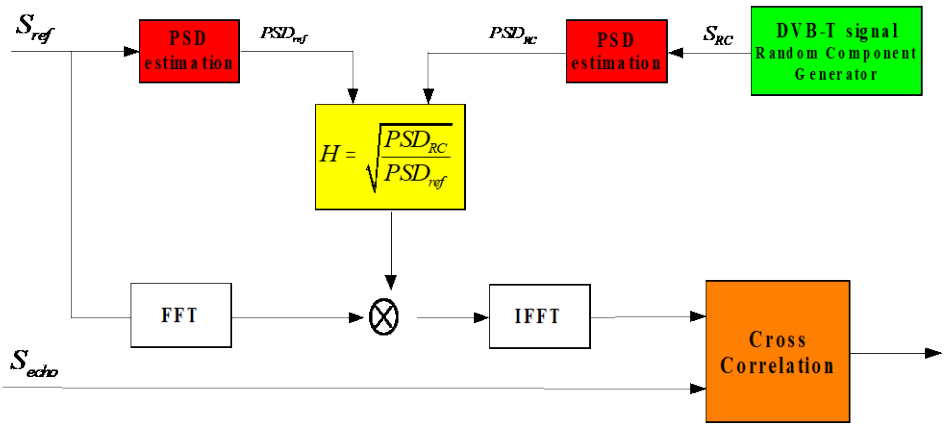


**Figure 3.6. Equalisation algorithm – functional block scheme**

The PSD is estimated for both the reference signal and for the locally generated signal (without pilot sequences). A filtering function *H* is then generated as the ratio of the two PSDs. The corrected PSD is obtained by multiplying the FFT of the reference signal by the function *H*. An IFFT is then applied to generate the spurious-free reference signal time sequence. An example of the effect of such an equalisation is shown in Fig. 3.7, where the zero-Doppler slice of the CAF along the range direction is shown before (blue line) and after

(red line) the equalisation process. The zero-range slice of the CAF along the Doppler direction is shown in Fig. 3.8 instead by using the same colour coding. Spurious peaks are visible in the zero-Doppler slice before the equalisation takes place. It is important to note that the main lobe is not distorted by this operation.

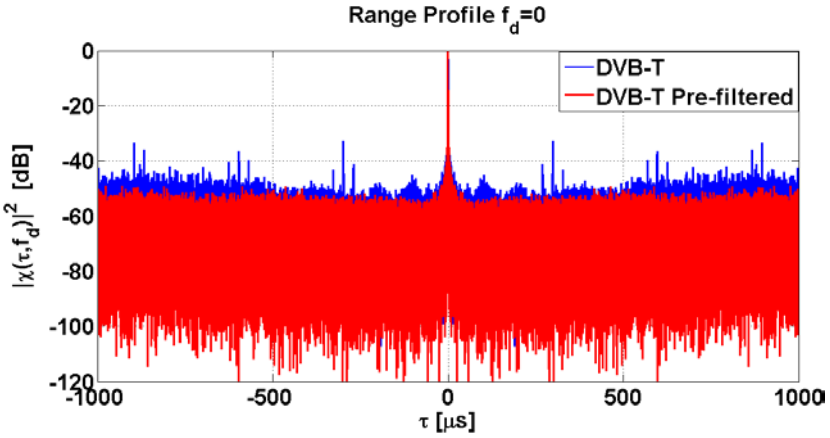


**Figure 3.7. Equalisation effect – CAF – Zero-Dopper slice along the range coordinate**

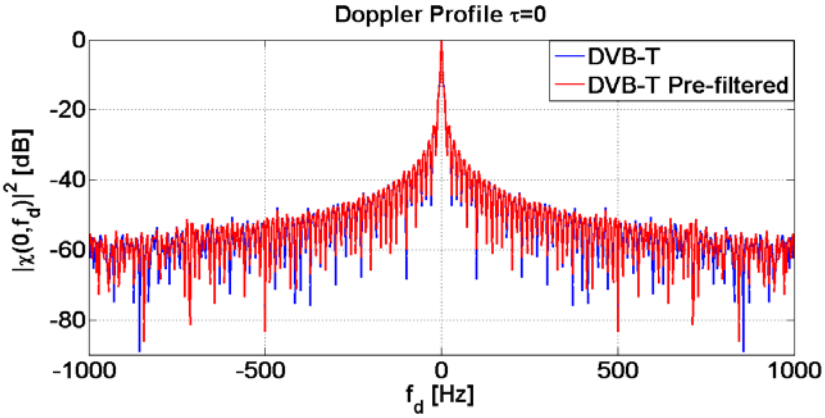


**Figure 3.8. Equalisation effect – CAF – Zero-range slice along the Doppler coordinate**

## 5.0 CONCLUSIONS

This notes are meant to provide some supporting material for the NATO Lecture Series SET-243 on Passive Radar Technology. They are not to be considered exhaustive or a full view of all the existing algorithms that have been conceived relatively to PCL.

## 6.0 REFERENCES

[1] Griffiths, H. D., and Baker, C. J., Passive coherent location radar systems. Part 1: performance prediction. IEE Proceedings Radar, Sonar and Navigation, 152, 3 (June 2005), 153–159.

[2] Howland, P. E., Griffiths, H. D., and Baker, C. J., Passive bistatic radar systems. In Bistatic Radar: Emerging Technology. Chichester, United Kingdom: John Wiley & Sons, 2008, ch. 7, 247–314

[3] Howland, P., *Editorial: Passive radar systems*, IEE Proceedings-Radar, Sonar and Navigation, 152 (June 2005), 105–106.

[4] Farina, A., and Kuschel, H., *Special Issue on Passive Radar (Part I)*, IEEE Aerospace and Electronic Systems Magazine, 27, 10 (2012).

[5] Malanowski, M., Mazurek, G., Kulpa, K., and Misiurewicz, J., *FM based PCL radar demonstrator*, In Proceedings of the International Radar Symposium, 2007.

[6] O'Hagan, D., Kuschel, H., Ummenhofer, M., Heckenbach, J., and Schell, J., *A multi-frequency hybrid passive radar concept for medium range air surveillance*, IEEE Aerospace and Electronic Systems Magazine, 27 (Oct. 2012), 6–15.

[7] H. Griffith, C. Baker, *Introduction to Passive Radar*, Artech House, 2017

[8] P. Lombardo, F. Colone, *Advanced processing methods for passive bistatic radar systems*, *in* Principles of Modern Radar – Vol. II, Scitech Publishing, 2013

[9] Petri, D., Moscardini, C., Martorella, M., Conti, M., Capria, A., and Berizzi, F., *Performance analysis of the batches algorithm for range-Doppler map formation in passive radar*, In Proceedings of the International Conference on Radar Systems (RADAR 2012).